Space-charge-limited current in nanowires

S. Alagha,[1] A. Shik,[2] H. E. Ruda,[2] I. Saveliev,[2] K. L. Kavanagh,[1] and S. P. Watkins[1]
[1]*Physics Department, Simon Fraser University, Burnaby, British Columbia V5A 1S6, Canada*
[2]*Centre for Advanced Nanotechnology, University of Toronto, Toronto, Ontario M5S 3E4, Canada*

(Received 27 February 2017; accepted 12 April 2017; published online 2 May 2017)

Space-charge-limited current is often observed in semiconductor nanowires due to carrier depletion and reduced electrostatic screening. We present a numerical study on geometric scaling of the space-charge-limited current in nanowires, in comparison with the thin film and bulk geometries, using an n^+-n-n^+-model. The model highlights the effects of the surroundings for thin films and nanowires and shows that the dielectric properties of the semiconductor have a negligible effect on the space-charge-limited transport for small dimensions. The distribution of equilibrium and injected charge concentration vary as the semiconductor dimensionality is reduced. For low doping, the ohmic current is controlled by charge diffusion from degenerate contacts rather than by the nanowire impurity concentration. The results of numerical calculations agree with a simple capacitance formalism which assumes a uniform charge distribution along the nanowire, and experimental measurements for InAs nanowires confirm these results. The numerical model also predicts that an asymmetric nanowire contact geometry can enhance or limit charge injection. *Published by AIP Publishing*. [http://dx.doi.org/10.1063/1.4982222]

I. INTRODUCTION

Space-charge-limited current (SCLC) is observed in materials with low free carrier concentration and ohmic contacts.[1] Semiconductors are an important class of materials that can be readily affected by space-charge effects. They can have low free carrier concentrations due to intrinsic or low doping as well as carrier depletion through surface trapping states in small dimensions. In the ideal case and in the absence of a potential drop at the contacts, and when the injected electron concentration is small compared to the equilibrium electron concentration n_0, the current density follows Ohm's law

$$J = en_0\mu\frac{V}{L}, \tag{1}$$

where V is the applied voltage, L is the separation between the contacts, and μ is a constant carrier mobility. However, the transport characteristics become non-linear at a cross-over voltage, V_x, where the injected charge begins to exceed the equilibrium charge. At this point, the electric field and charge distribution become non-uniform and depend on the sample geometry. Figure 1 shows schematics of bulk, thin film, and nanowire (NW) n^+-n-n^+-models to be compared in Section II.

The analytical solution for SCLC characteristics in bulk geometries, where the contact dimensions are large compared to the length of the structure, as shown in Fig. 1(a), is known as the Mott-Gurney-Law[2,3]

$$J = \frac{9}{8}\epsilon_0\epsilon_r\mu\frac{V^2}{L^3}, \tag{2}$$

where ϵ_0 is the permittivity of free space and ϵ_r is the relative permittivity of the bulk material.

The SCLC theory for low-dimensional systems (thin films and nanowires) differs from that of bulk samples in that the electric field of the space-charge is concentrated mostly outside the semiconductor due to the fact that screening effects are suppressed.[4–6] In this case, the field distribution outside the thin film or nanowire is found by solving the Laplace, rather than Poisson, equation, and the solution depends on the dielectric constant of the surroundings, rather than the semiconductor. This means that surroundings with different dielectric properties than the semiconductor have a profound impact on charge transport inside the structure.

For thin films, the contact area and material volume are reduced in one dimension leaving charge restricted to a film thickness D much smaller than L, as shown in Fig. 1(b). An analytical solution for SCLC in two-dimensional thin films was given[7] and further studied and verified with numerical calculations[8] as

$$J = \zeta\epsilon_0\epsilon_r\mu\frac{V^2}{L^2D}, \tag{3}$$

where ϵ_r is the dielectric constant of the film and its surroundings, and ζ is a numerical constant of order unity that depends on the contact geometry. Charge injection depends on the film thickness and is higher compared to a bulk structure with the same length due to decreased screening.

In the case of nanowires with a cylindrical shape with length L and radius r (Fig. 1(c)), where $L \gg r$, the screening of charge is further reduced. An analytical solution of SCLC for the nanowire geometry was calculated[9] for point contacts

$$J = \zeta_0\epsilon_0\epsilon_r\mu\frac{V^2}{r^2L}, \tag{4}$$

where ϵ_r is the dielectric constant of the nanowire and its surroundings, and ζ_0 is a numerical constant of order unity.

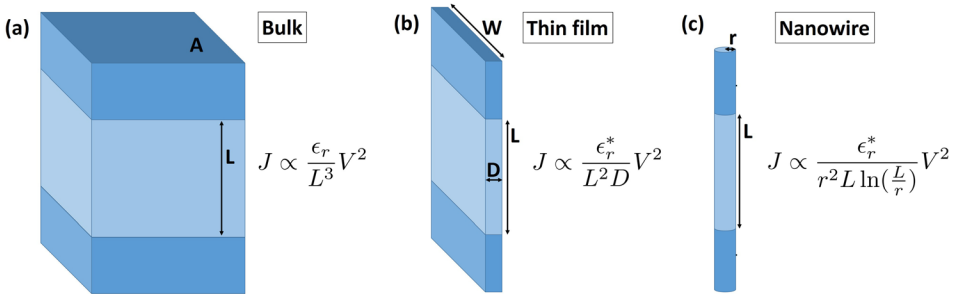

FIG. 1. Schematic of (a) bulk, (b) thin film, and (c) nanowire n^+-n-n^+-models with geometric proportionality of the current density.

We can estimate the nanowire J-V dependence using a simple formalism where the injected charge per unit area $Q_{inj} = CV$ is given by the capacitance C.[2,10] This approach is not exact since the concentration distribution in the presence of current is non-uniform. In bulk samples, where the exact solution is given by Eq. (2), this non-uniformity was shown[2] to change the answer only by a numerical factor of order unity. In nanowires, where the charge profile is smooth due to weak screening, we can assume a similar accuracy with this approach. For nanowires, the capacitance is approximately given by a uniformly charged elongated ellipsoid[11]

$$C \approx \epsilon_0 \epsilon_r^* \frac{L}{\pi r^2 \ln(L/r)}, \tag{5}$$

where ϵ_r^* is the dielectric constant of the surrounding medium rather than the nanowire. The current density is then defined by the nanowire geometry and its surrounding dielectric, and the only relevant intrinsic parameter is the semiconductor mobility μ

$$J = \frac{Q_{inj}}{t} = \frac{C\mu}{L^2} V^2 \approx \epsilon_0 \epsilon_r^* \mu \frac{V^2}{\pi r^2 L \ln(L/r)}. \tag{6}$$

To summarize, approximate analytical calculations for bulk, thin film, and nanowire systems show that for high V, when Ohmic conductivity caused by equilibrium carriers is negligible, the quadratic dependence $J \propto V^2$ has universal character while the length dependence of the current density is determined by the sample dimensionality.

In this paper, we present results of a numerical study on SCLC characteristics of bulk, thin film, and nanowire geometries. Equations (2)–(4) represent approximate analytical expressions, where diffusion currents were neglected. Our numerical simulations allow the consideration of problems, not only with different dimensionality in the framework of a single approach, but also take into account the difficult, if not impossible, aspects for analytical consideration, namely: (i) contribution of diffusion current, (ii) realistic contacts with a finite doping level, and (iii) enhancement of equilibrium electron concentration due to weak screening in low-dimensional systems. We confirm the relationship $J \propto V^2$ and the enhancement of SCLC due to the nanowire aspect ratio with a geometry factor that agrees with the simple capacitance model (Eq. (6)). Furthermore, we show the effect of the nanowire surrounding dielectric and the influence of contact geometry. Finally, we apply the model to an example of experimental measurements in InAs nanowires and discuss the extraction of carrier concentration and mobility.

II. NUMERICAL METHOD AND MODEL

Simulations were carried out with the semiconductor module in COMSOL Multiphysics 5.2, a commercially available software that uses finite element methods. The software package includes predefined interfaces and domain models simulating semiconductor physics. It solves Poisson's and current continuity equations for drift and diffusion, however, does not include tunneling, quantum confinement, and surface states.

Prior to simulations for the nanowire geometry, we studied bulk and thin film geometries and verified the analytical solutions given by Eqs. (2) and (3). For all geometries, an n^+-n-n^+-model was set up, following the numerical model and parameters introduced for thin films.[8] The contacts were degenerately n-type, with donor concentration, $N_d^{contacts} = 10^{19}\,\mathrm{cm}^{-3}$, and provided an electron reservoir to the lightly n-type doped structure with donor concentration, $N_d = 10^{12}\,\mathrm{cm}^{-3}$. Complete donor ionization and continuous Fermi levels at the n^+-n-interfaces were assumed. An ohmic metal interface was placed on the outside of both n^+-contacts, where one contact side was grounded and a variable voltage was applied to the other side. All structures had a relative dielectric constant, $\epsilon_r = 10$, field-independent mobility, $\mu = 1000\,\mathrm{cm}^2/\mathrm{Vs}$, and temperature, $T = 300\,\mathrm{K}$, and were under steady-state conditions.

Thin films and nanowires were surrounded by a dielectric medium where no current flow was allowed. This feature is crucial to the study since the electric field created by injected charge is primarily located outside the semiconductor for low-dimensional systems. Hence, the potential distribution is to be found from the Laplace equation outside the semiconductor. The dielectric constant of the surroundings was initially set to that of the thin film or nanowire for geometry studies and varied to investigate its effect on charge injection properties.

Thin films were studied with a strip contact geometry where the contact thickness was equal to the film thickness and its length much larger than the film. The film length was 5 μm, and the thickness was varied between 0.01 μm and 100 μm. The nanowire geometry was assumed to be a cylinder and modeled through a two-dimensional simulation with rotational symmetry. Figure 2 presents diagrams of the different nanowire contact geometries used in this work: (a) strip contacts, (b) large contacts, and (c) a combination of strip and large contacts. The effect of the nanowire aspect ratio at equilibrium and with applied voltage was studied with the strip contact geometry. The nanowire length was 5 μm, and the radius was varied between 0.05 μm and 5 μm.

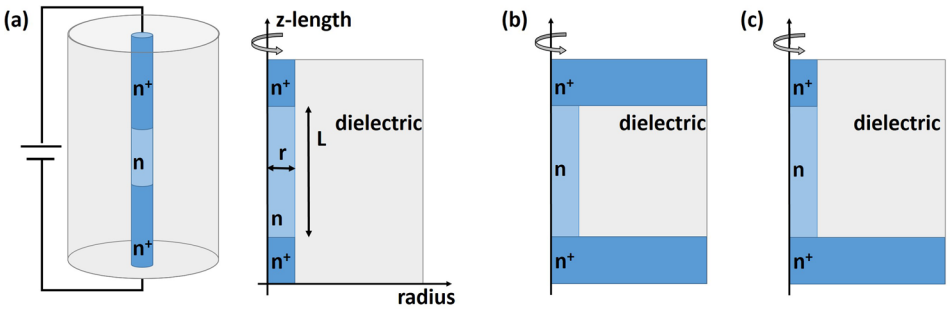

FIG. 2. Schematic of cylindrical nanowire models with (a) strip contacts, (b) large contacts, and (c) a combination of strip and large contacts.

In addition, the effect of large contacts, which exceed the nanowire radius, and asymmetric contacts on SCLC was studied and considered in the discussion of the experimental data.

III. SIMULATION RESULTS

A. Bulk and thin film model

Figure 3(a) shows a plot of the simulated equilibrium carrier concentration, $n(x)$, in a bulk n^+-n-n^+-model as a function of position between the contacts. Charge diffusion from the more heavily doped n^+-regions occurs into the lightly doped n-region and is eventually opposed by a built-in electric field. This leads to an excess space-charge in the lightly doped region even at zero bias. The excess charge from both contacts overlaps such that the total free carrier concentration is greater than the donor concentration, and increases with decreasing length. Figure 3(b) shows the simulated $n(L/2)$ as a function of length on a double-logarithmic scale. The free carrier concentration varies inversely with the square of the length for $n(L/2) \gg N_d$ and saturates towards N_d for large L.

This effect has been studied analytically and observed experimentally.[12,13] The exact solution for the free carrier concentration halfway between the contacts, where it drops to a minimum in bulk, is

$$n(L/2) = \frac{2\pi^2 \epsilon_0 \epsilon_r kT}{eL^2} \propto \frac{\epsilon_r}{L^2}, \tag{7}$$

where ϵ_r is the permittivity of the material, k is the Boltzmann constant, and T is the temperature.[12] The dependence of geometry on the diffusion at the n^+-n-interfaces can also be estimated with a simple capacitance model. The total charge concentration at equilibrium is $n = Q/eL = CV_b/eL$, where V_b is the built-in voltage of the n^+-n-structure. Inserting the parallel plate capacitance for the bulk geometry leads to $n \approx \epsilon_0 \epsilon_r V_b / eL^2$, with the same geometric scaling as the analytical solution (Eq. (7)).

It follows that the ohmic current density, when $n_0 \approx n(L/2)$ for $n(L/2) \gg N_d$, can be found by substituting Eq. (7) into Eq. (1), giving

$$J \approx 2\pi^2 \epsilon_0 \epsilon_r \mu kT \frac{V}{L^3} \propto \frac{\epsilon_r}{L^3}. \tag{8}$$

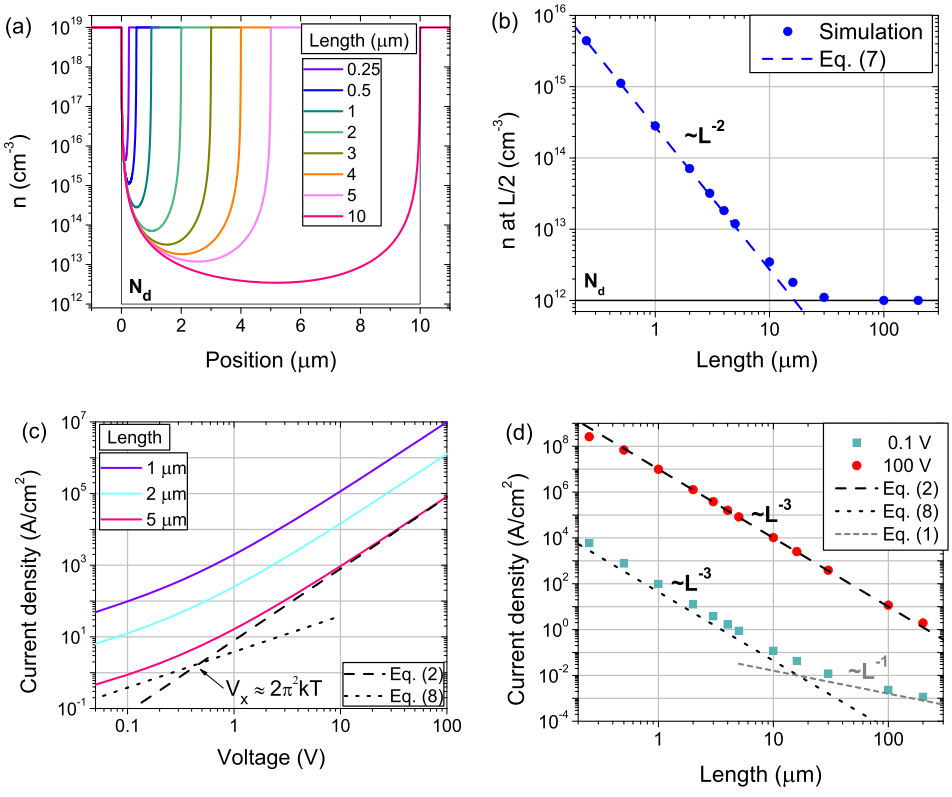

FIG. 3. Bulk model simulation results: (a) Equilibrium carrier concentration, $n(x)$, for different contact separations, as a function of position. (b) Lowest concentration, $n(L/2)$, between the contacts as a function of length. Current density as a function of (c) voltage for different length, L, and (d) length at fixed voltages.

This current has the same geometrical scaling factor as the SCLC. However, Eq. (8) underestimates the ohmic current since the average free carrier concentration is higher than given by Eq. (7). The free carrier concentration is a function of distance and is higher near the contacts.

Figure 3(c) shows the simulated current density as a function of voltage for different lengths ($L = 1-5\ \mu$m). The dashed and dotted lines correspond to the Mott-Gurney-Law (Eq. (2)) and Ohm's Law (Eq. (8)), respectively. The current density as a function of voltage increases overall with decreasing length but the crossover voltage V_x stays constant at the indicated value. The free carrier concentration is greater than the intrinsic doping concentration over the whole voltage range, due to drift-diffusion of charge at the n^+-n-interfaces at equilibrium and small bias, and due to charge injection at large bias. Figure 3(d) is a plot of current density at small voltage (0.1 V, ohmic region) and large voltage (100 V, SCLC region) as a function of length. The SCLC scales with the same geometric factor for all lengths. However, the ohmic current shows a change in length exponent when the free carrier concentration approaches the doping concentration, $n(L/2) \approx N_d$. The cross-over voltage where ohmic current changes to SCLC is often used to extract the free carrier concentration, $V_x = en_0L/C$.[3] The simulation results show that when interpreting the value of n deduced from V_x, it is important to investigate the dependence of geometry on the J–V characteristics in order to determine whether the free carrier concentration is controlled by the doping concentration ($n_0 = N_d$) or by diffusion from the contacts ($n_0 \approx n(L/2)$).

Figure 4(a) shows the equilibrium carrier concentration in an n^+-n-n^+-model for thin films as a function of position, for a fixed length $L = 5\ \mu$m, and shows a strong increase in carrier concentration with decreasing film thickness. Figure 4(b) plots the equilibrium carrier concentration halfway between the contacts as a function of thickness D for a dielectric constant $\epsilon_r^{outside} = 1$ and 10. The value for a bulk structure with $L = 5\ \mu$m is also presented (Eq. (7)). The carrier concentration converges to the bulk value for thicknesses much larger than the length (in this case 5 μm) and increases with decreasing thickness by $1/D$. Moreover, a larger dielectric constant in the surrounding medium leads to higher carrier concentration, where the change is nearly linear. Based on a simple scaling argument beginning from the bulk (Eq. (7)), we can estimate the minimum value of the carrier concentration between the contacts as

$$n(L/2, D) \propto \frac{\epsilon_r^*}{LD} \tag{9}$$

for thin films, where the geometry factor is given by $1/LD$ and ϵ_r^* is the dielectric constant of the material surrounding the film. Thus, the ohmic current at low voltages increases for thin films with $n(L/2, D)$ for $n(L/2, D) \gg N_d$. Figure 4(c) shows the J-V characteristics, increasing with decreasing thickness over the whole voltage range. This leaves the cross-over, from ohmic current to SCLC, constant, similar to the bulk case. The SCLC is extracted for a uniform dielectric constant $\epsilon_r = 10$ throughout the model and $\epsilon_r^{outside} = 1$ as a function of film thickness in Fig. 4(d), and normalized to the expected bulk value (Eq. (2)). The effect of the surrounding dielectric becomes significant when the film thickness is comparable to the film length and smaller. We can modify the analytical solution for SCLC in thin films[8] (Eq. (3)) by changing ϵ_r to ϵ_r^* which is the dielectric constant of the surroundings rather than the film, resulting in

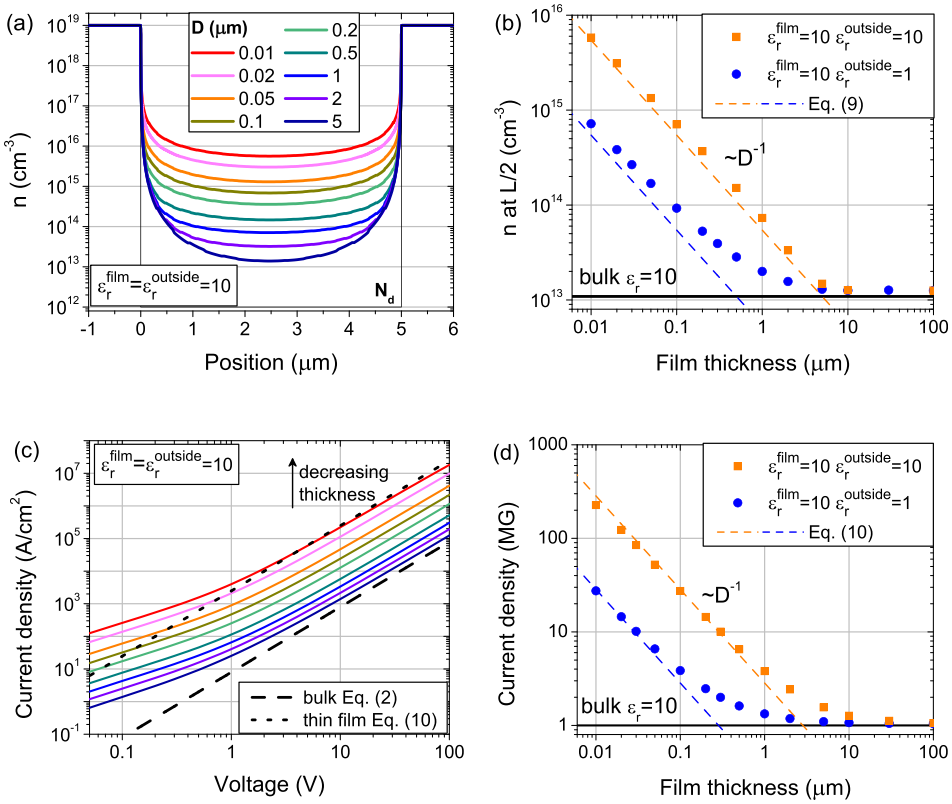

FIG. 4. Thin film model simulation results: Equilibrium carrier concentration (a) as a function of position for several film thicknesses, D, and (b) at L/2 as a function of film thickness. Current density as a function of (c) voltage and (d) film thickness.

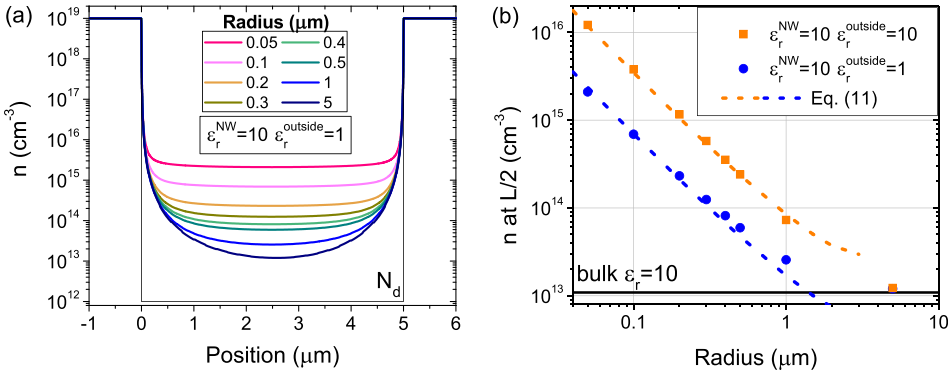

FIG. 5. Nanowire (NW) model simulation results: Equilibrium carrier concentration as a function of (a) position, x, from the bottom contact for different radii, total length $L = 5\,\mu$m, and (b) at L/2 as a function of nanowire radius, and outside dielectric constant.

$$J = \zeta \epsilon_0 \epsilon_r^* \mu \frac{V^2}{L^2 D}. \tag{10}$$

This has been overlaid with the simulated results in Figs. 4(c) and 4(d).

In summary, the electric field of charges in smaller structures extends to a range larger than the thickness where no charges are present. This leads to less coulombic interaction and screening of charge and allows more charge per unit volume in the film at equilibrium and with applied voltage.

B. Nanowire model at thermal equilibrium

Figure 5(a) presents the equilibrium carrier concentration in an n^+-n-n^+-model for nanowires as a function of position from the bottom contact, where the dielectric constant of the surrounding is $\epsilon_r^{outside} = 1$. The length of the nanowire is fixed at $L = 5\,\mu$m, but the radius is varied. The carrier diffusion from both contacts overlaps in the nanowire and its free carrier concentration is greater than the donor concentration, increasing with decreasing nanowire radius. Since electron screening in low-dimensional systems is strongly suppressed and not characterized by some definite screening length, the regions of high equilibrium electron concentration penetrate far from the heavily doped contacts. Figure 5(b) plots the minimum carrier concentration between the contacts as a function of nanowire radius for a dielectric constant 1 and 10 of the surrounding medium. The equilibrium carrier concentration agrees well with the bulk model (Eq. (7)) for the largest radius, which is comparable to the nanowire length and increases for smaller radii. Similar to thin films, the carrier concentration is higher for a larger dielectric constant of the surrounding medium such that the effect of the nanowire dielectric constant becomes negligible. As discussed previously, the effect of nanowire geometry on equilibrium carrier concentration can be estimated from the capacitance (Eq. (5)), giving

$$n(L/2, r) \propto \frac{\epsilon_r^*}{r^2 \ln(L/r)}, \tag{11}$$

where ϵ_r^* is the dielectric constant of the outside material. This proportionality is represented by the dashed lines in Figure 5(b), where a numerical prefactor was adjusted to match the simulations.

Figure 6 shows potential contour lines and arrows representing the direction and magnitude of the electric field for nanowires with radius $r = 1\,\mu$m and $r = 0.1\,\mu$m. The component of the electric field parallel to the nanowire becomes weaker for smaller nanowires whereas the perpendicular component is stronger. Hence, less electric field is opposing the diffusion of electrons from the highly doped contacts into the smaller nanowires.

C. Nanowire model under bias

When the nanowire is under bias, the carrier injection profile changes drastically with the aspect ratio, similar to the equilibrium situation. Figure 7(a) shows the carrier concentration for different radii as a function of position from the bottom contact at large bias (10 V) where SCLC is dominating. The profile follows $n(x) \propto x^{-1/2}$ as predicted by the Mott-Gurney[2] results for bulk structures when the nanowire radius becomes comparable to its length. For decreasing radius, the injected charge density is higher and more uniformly distributed along the nanowire with a dip near the charge extracting contact. Figure 7(b) presents the magnitude of the electric field component along the length of the nanowire at large bias. For a radius comparable to the length, the electric field follows the predicted bulk dependence, $E(x) \propto x^{1/2}$. For nanowires with smaller radii, the electric field is flatter along the nanowire and shows a larger increase at the charge extracting contact.

Figure 7(c) plots the simulated current density as a function of voltage. At low bias, the current is ohmic, $J \propto V$, determined by the equilibrium carrier concentration and increases with decreasing nanowire radius as $n(L/2, r)$ (Eq.

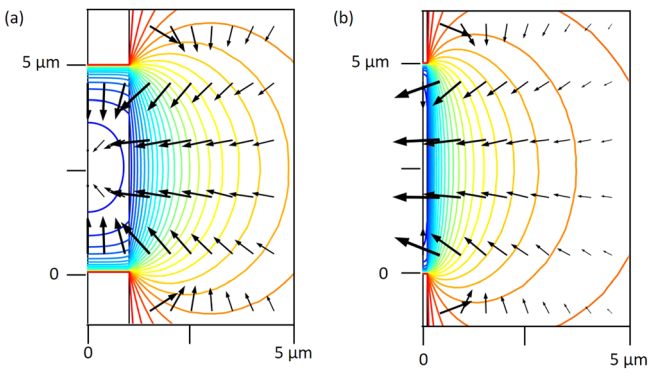

FIG. 6. Contour lines of equipotentials and arrows indicating the direction and magnitude of the electric field for nanowire models with radius (a) $r = 1\,\mu$m and (b) $r = 0.1\,\mu$m.

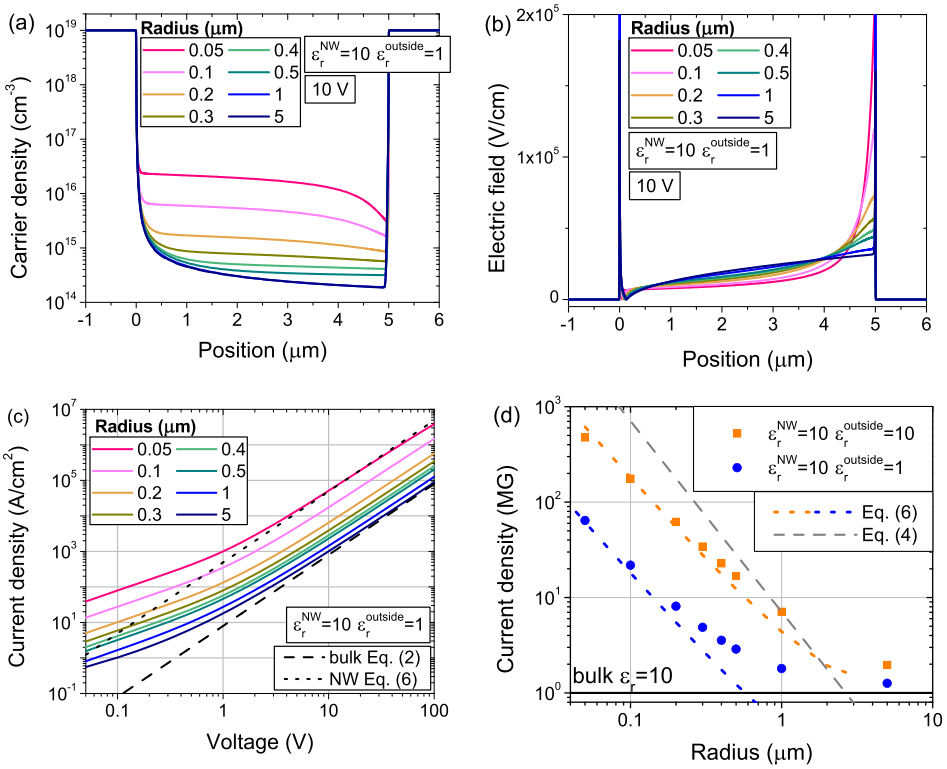

FIG. 7. Nanowire model simulation results: Plots of (a) carrier concentration and (b) electric field as a function of position at large bias for radii from 0.05 to 5 μm. Plot of (c) current density as a function of voltage. Dashed and dotted lines present Eq. (2) for bulk and Eq. (6) for a nanowire with radius 0.05 μm. (d) Current density at large bias as a function of radius, and outside dielectric constant.

(11)). The high voltage region is space-charge-limited, $J \propto V^2$, and saturates to the Mott-Gurney-Law (dashed line) for the largest radius and increases with decreasing radius, following Eq. (6) (dotted line) in the limit of thin nanowires. Both the ohmic and space-charge components have the same geometrical dependence for small radii, leaving the crossover voltage constant. Figure 7(d) plots the current density at a fixed large bias where space-charge controls the current transport as a function of nanowire radius for a surrounding dielectric medium with permittivity equal to 1 and 10, respectively. The current density is normalized to the corresponding bulk value determined by the Mott-Gurney-Law. It approaches the bulk value for large radii and increases proportional to $1/r^2L\ln(L/r)$ for smaller radii (dotted lines). This geometric factor agrees with the simple formalism of a uniformly charged ellipsoid (Eq. (6)) and differs from a previously published analytical solution calculated for point contacts, which scales as $1/r^2L$ (dashed line, Eq. (4)).[9] Also, Fig. 7(d) illustrates an important point that the current density is approximately proportional to the dielectric constant of the surrounding medium, while the nanowire's dielectric constant becomes negligible. The electric field in smaller structures decays over a range larger than the radius, and extends to where no charges are present. This leads to less coulombic interactions, i.e., reduced screening of charge, and allows more charge per unit volume in the nanowire. In addition, a larger dielectric constant on the outside of the nanowire leads to a higher polarization of the dielectric which further reduces the electric field inside the nanowire.

D. Comparison of bulk, thin film, and nanowire models

Figure 1 showed a schematic of bulk, thin film, and nanowire models. Figure 8 shows a comparison of their electron concentrations, electric fields, and current densities. In this comparison, all structures have the same length $L = 5\ \mu$m, mobility $\mu = 1000\ \text{cm}^2/\text{Vs}$, and doping concentration $N_d = 10^{12}\ \text{cm}^{-3}$. The thin film has a reduced thickness $D = 0.2\ \mu$m, and the nanowire has a radius $r = 0.1\ \mu$m. Solid lines present simulations with a uniform dielectric constant $\epsilon_r = \epsilon_r^* = 10$ throughout the model. Dashed lines consider the effect of air surrounding the thin film and nanowire with $\epsilon_r^* = 1$. Figure 8(a) shows the equilibrium carrier concentration as a function of position between the contacts. Clearly, the carrier concentration is overall higher and distributed more uniformly along the structure with decreasing dimensionality. Excess charge from the degenerate contacts entering the material is more effectively screened in bulk structures. Thin films and nanowires show less screening due to the restricted geometry. Similarly, when a large bias is applied, the injected charge concentration is larger for thin films and nanowires compared to bulk, which is shown in Fig. 8(b). For bulk, the charge concentration is clearly higher near the injecting contact and drops over the length of the structure.[2] The injected charge is more uniformly distributed, and the charge profile along the structure significantly changes with decreasing dimensionality due to reduced carrier screening in low-dimensional structures.[8] The component of the electric field parallel to current flow increases near the charge extracting contact but drops within the structure for thin films and nanowires, which is plotted in Fig. 8(c). The current density (Fig. 8(d)) increases overall with decreasing dimensionality. At low bias, where thermal carriers dominate the current transport, this is due to higher charge diffusion from the contacts leading to a higher equilibrium carrier concentration and at large bias this is due to higher charge injection and

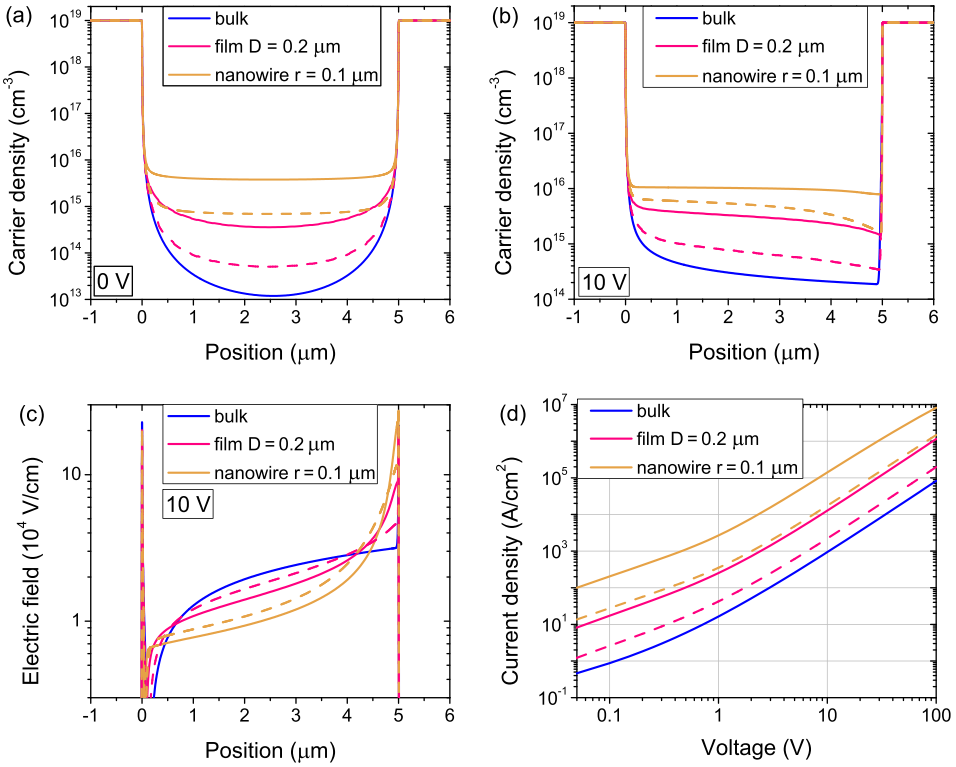

FIG. 8. Comparison of bulk, thin film, and nanowire models: (a) equilibrium carrier concentration, (b) injected carrier concentration, and (c) magnitude of electric field at 10 V, and (d) current density. Solid lines are characteristics for constant permittivity $\epsilon_r = 10$ throughout the model, and dashed lines show the effect of the surrounding dielectric, $\epsilon_r^* = 1$.

modified electric field profile. The free carrier concentration at equilibrium is determined by dielectric and geometric properties when the doping concentration is low. In this case, both ohmic and SCLC transport characteristics scale with the same geometric factors that are summarized in Fig. 1. For higher doping concentrations, the equilibrium carrier concentration stays constant and does not depend on the geometry such that the cross-over from ohmic currents to SCLC would be dependent on geometry.

E. Effect of nanowire contact geometry

As discussed in Section III A–D, the electric field surrounding nanowires has a strong influence on charge diffusion at equilibrium and charge injection with applied voltage. The geometric details of the contacts to the nanowires strongly affect the electric field and consequently the current characteristics. Nanowires are commonly grown perpendicular to the substrate surface and completely surrounded by air. In this case, they can be directly contacted with a small area probe from the top while the substrate acts as a second contact, thus potentially creating an asymmetric contact geometry.[14,15] Another method is that the area between the nanowires is filled with a dielectric material and a single large contact is made to the top of all nanowires without taking them off the growth substrate, such that they are all connected in parallel.[16,17]

Figure 2 showed schematics of the nanowire model with (a) strip contacts on both sides, (b) large contacts on both sides, and (c) strip contact on one side and large contact on the other side. Figure 9 shows current density as a function of voltage on a linear scale in (a) and double-logarithmic scale in (b) for a nanowire with length $L = 5\ \mu$m and radius $r = 0.1\ \mu$m for these three contact geometries. Symmetric contacts lead to symmetric current characteristics for positive and negative voltage. A cross-over from ohmic to space-charge-limited current is observed for symmetric strip or large area contacts. Despite the different geometry, the current is very similar for these symmetric configurations. In contrast, the current characteristics are asymmetric for asymmetric contacts. The voltage is applied at the strip contact side for this case, and the large contact is grounded. A positive voltage corresponds to electron injection from the large contact and a negative voltage corresponds to electron injection from the strip contact. When a positive/negative voltage is applied to the strip contact, the current density is overall lower/higher compared to the symmetric contact cases. Charge injection from the strip contact is enhanced, while charge injection from the large contact is suppressed. These asymmetric characteristics are most profound for nanowires with a large aspect ratio and disappear when the radius is comparable to the length. Figures 9(c) and 9(d) show the carrier concentration as a function of position between the contacts for positive and negative 10 V applied to the right side contact for all three contact geometries. For comparison, the equilibrium concentration for the asymmetric configuration is plotted as a dashed line. The carrier concentration is overall higher and more uniform for asymmetric contacts compared to symmetric contacts when charge enters the nanowire through the strip contact. Through the large contact sides, the carrier concentration increases only slightly over the equilibrium value on the injecting side and shows depletion on the opposite contact.

The influence of contact geometry on the electrical transport in nanowires has been studied widely and effects such as increase in contact resistivity[18] and distribution of electron concentration[19] have been reported. Similar asymmetric trends for current characteristics were predicted for semiconductor nanowires including field-dependent mobilities.[20] Our study confirms the importance of geometry

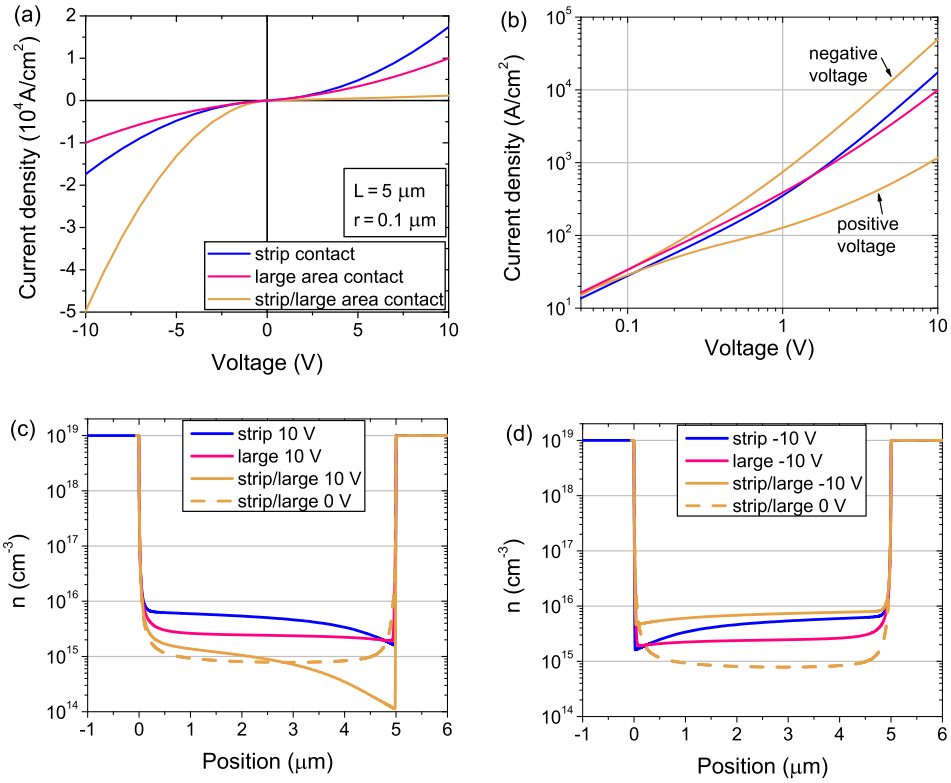

FIG. 9. Current density as a function of voltage for symmetric and asymmetric nanowire contact geometries on (a) linear and (b) double-logarithmic scale. Carrier concentration as a function of position for (c) positive and (d) negative voltage applied to the right side, for symmetric and asymmetric contacts.

effects for nanowires and its influence on space-charge-limited current. These characteristics could be mistaken for rectifying properties in electrical measurements and misleading charge transport interpretations.

IV. COMPARISON OF SIMULATIONS WITH EXPERIMENTAL DATA

The preceding results from simulation of charge diffusion and injection in nanowires as a function of aspect ratio and contact geometry are for ideal materials and interfaces. Experimental measurements often show a superposition of distinct electrical transport mechanisms and need careful interpretation. The simulation results predict carrier concentrations higher than the doping concentration at equilibrium and hence larger ohmic currents for smaller nanowires due to charge diffusion from degenerate contacts. Experimentally, the current at small voltages is influenced and perhaps limited by the interface resistance depending on contact material, fabrication, and measurement method. Space-charge-limited current dominates at higher bias when interface barriers are negligible and the injected charge exceeds the equilibrium charge. In that regime, the contact interface resistances have little influence; however, the contact geometry can play an important role, since it influences the electric field surrounding the nanowire. These effects need to be considered when extracting material parameters such as resistivity, mobility, and intrinsic carrier concentration from J-V measurements. In principle, the mobility can be extracted from the SCLC region and the free carrier concentration from the cross-over of ohmic to space-charge-limited transport. Our simulation results suggest that the free carrier concentration is determined by geometry, rather than intrinsic properties, for nanowires with low doping. In this case, the extracted free carrier concentration from the cross-over voltage would not represent the doping concentration but the effective carrier concentration. Moreover, the numerical results suggest that the nanowire dielectric constant has negligible influence, since the electric field is mainly located outside the nanowire. Therefore, the SCLC characteristics for nanowires of different materials with a similar size and mobility can be expected to be the same.

Space-charge-limited current has been reported in several semiconductor nanowire materials with different contact geometries.[9,21–23] In this work, we measured undoped, wurtzite InAs, (0001) oriented nanowires. Figure 10(a) shows an SEM image of an InAs nanowire, with $L = 1.5\,\mu$m and $r = 25$ nm, being contacted by a tungsten (W) nanoprobe. The nanowires were grown by solid-source molecular beam epitaxy via Au catalyst nanoparticles on Si-doped (111)B n-GaAs ($n = 10^{18}\,\text{cm}^{-3}$) substrates at 400 °C. Electrical measurements were carried out *in situ* on individual nanowires using a fixed W-nanoprobe mounted inside an SEM. The W-tip was cleaned using a Ga focused ion beam in the same SEM. The top contact was achieved by moving the Au particle of a nanowire underneath the W-nanoprobe. A large area In contact on the backside of the substrate served as the bottom contact. The current-voltage characteristics at room temperature were obtained by applying a voltage and measuring the current. During the electrical measurements, the SEM electron source was blocked.

Figures 10(b) and 10(c) show the experimental and simulated J-V curves for the InAs nanowire shown in (a) on a linear and double-logarithmic scale. The experimental curves are symmetric, with $J \propto V$ at small voltages and $J \propto V^2$ at larger voltages, characteristic of SCLC. The measured J-V behavior

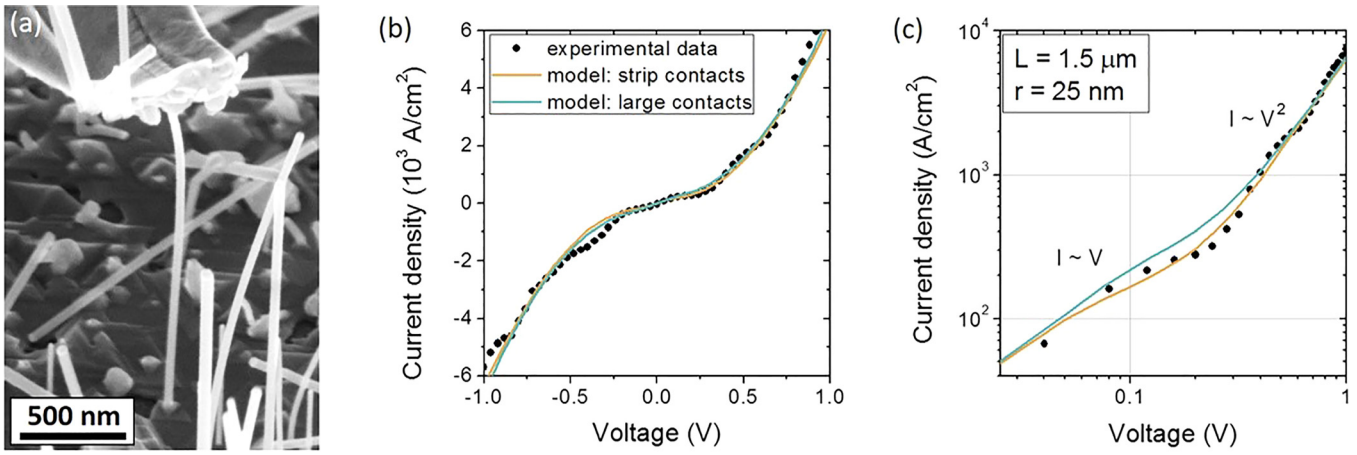

FIG. 10. (a) Tungsten-nanoprobe contacting a single undoped InAs nanowire inside an SEM. *J-V* measurement and model with strip and large contacts on (b) linear and (c) double-logarithmic scale.

cannot be explained by Schottky barriers at the contacts since the curves were symmetric and contain no exponential or sub-linear portions. The low resistance, ohmic properties of the In contact at the substrate backside were confirmed by W-probing a large area In contact connected directly onto the heavily doped n-GaAs substrate. The heterojunction at the epitaxial InAs nanowire/n-GaAs interface is also expected to be an ohmic, tunnel junction at room temperature. Similarly, the W/Au interface resistance was measured by contacting the W-nanoprobe to Au nanoparticles deposited directly onto the n-GaAs substrate, which confirmed a negligible contact resistance compared to that of the InAs nanowires.

Furthermore, the symmetry in the measured *J-V* characteristics suggests a symmetric ambient electric field created by the contacts. The probe is much larger than the nanowire leading to an almost flat contact at the top as well as the bottom. However, symmetric transport curves have also been observed for less symmetric probe geometries.[21,24] The measured *J-V* curves are ohmic at small voltages and show a cross-over to SCLC at $V_x = (0.25 \pm 0.05)$ V. The free carrier concentration can be estimated from V_x by

$$n = \frac{\epsilon_0 V_x}{e\pi r^2 \ln(L/r)}, \tag{12}$$

where Eqs. (1) and (6) have been equated, and lead to $n \approx 10^{15}\,\mathrm{cm}^{-3}$. We used the nanowire dimensions $L = 1.5\,\mu$m and $r = 25$ nm in our models for symmetric strip or large contacts to extract the free carrier concentration and mobility, where the nanowire was surrounded by air. Both models suggested free carrier densities $n \approx 10^{16}\,\mathrm{cm}^{-3}$ in the nanowire due to excess charge from the degenerate contacts (as discussed in Section III B). However, this is an order of magnitude higher than the value just calculated from V_x. In order to reduce the calculated free carrier concentration such that the modeling results fit the experimental currents at low bias, we added compensating acceptors. Experimentally, the lower free carrier concentration or larger resistance at low bias could be due to contact resistances, surface and bulk electron traps or radially non-uniform conduction. The solid lines in Figs. 10(b) and 10(c) are simulations that reproduce the experimental data. The carrier concentration and mobility are $n = 1 \times 10^{15}\,\mathrm{cm}^{-3}$ and $\mu = 1500\,\mathrm{cm}^2/\mathrm{Vs}$ for the strip-contact model and $n = 2 \times 10^{15}\,\mathrm{cm}^{-3}$ and $\mu = 2000\,\mathrm{cm}^2/\mathrm{Vs}$ for the large-contact model. These parameters are comparable to previously reported values for similarly grown undoped InAs nanowires measured by field-effect transistor techniques.[25,26] The comparison of our simulation model and experimental data shows that SCLC becomes important in nanowires with low free carrier concentration ($<10^{16}\,\mathrm{cm}^{-3}$). For nanowires with higher free carrier concentration ($>10^{17}\,\mathrm{cm}^{-3}$), due to doping or surface accumulation, SCLC might not be observed since the cross-over voltage would be at larger voltages and possibly not reached experimentally.

V. CONCLUSIONS

We have studied SCLC in semiconductor nanowires using an n^+-n-n^+ finite element model. A simple analytical estimate was derived for SCLC in nanowires and shown to be in good agreement with the geometric trends of the modeling results at high charge injection. The reduced carrier screening of the nanowire geometry leads not only to enhanced charge injection under bias but also to enhanced equilibrium carrier density. For low doping, this can lead to a cross-over voltage between ohmic and SCLC behavior that is independent of the doping concentration. The relative dielectric constant of the surroundings is shown to have a large effect on the equilibrium and *J-V* characteristics of semiconductor thin films and nanowires. A larger dielectric constant of the surroundings leads to higher charge diffusion at equilibrium and higher charge injection with applied bias such that the dielectric constant of the semiconductor has little effect. Modeling results predict that asymmetry in the contact geometry can result in significant asymmetry in the *J-V* characteristics. The model was used to accurately fit experimental *J-V* measurements for InAs nanowires.

ACKNOWLEDGMENTS

We are grateful to NSERC for partial funding of this work. We also acknowledge the support of 4D LABS Nanoimaging staff and CMC Microsystems.

[1]M. A. Lampert and P. Mark, *Current Injection in Solids* (Academic Press, 1970).
[2]N. F. Mott and R. W. Gurney, *Electronic Processes in Ionic Crystals* (Clarendon Press, Oxford, 1948).
[3]M. A. Lampert, Rep. Prog. Phys. **27**, 329 (1964).
[4]T. Ando, A. B. Fowler, and F. Stern, Rev. Mod. Phys. **54**, 437 (1982).
[5]F. Léonard and J. Tersoff, Phys. Rev. Lett. **83**, 5174 (1999).
[6]S. G. Petrosian and A. Y. Shik, Sov. Phys. JETP **69**, 1261 (1989), ISSN 0038-5646.
[7]J. A. Geurst, Phys. Status Solidi **15**, 107 (1966).
[8]A. A. Grinberg, S. Luryi, M. R. Pinto, and N. L. Schryer, IEEE Trans. Electron Devices **36**, 1162 (1989), ISSN 0018-9383.
[9]A. A. Talin, F. Léonard, B. S. Swartzentruber, X. Wang, and S. D. Hersee, Phys. Rev. Lett. **101**, 076802 (2008).
[10]A. Rose, Phys. Rev. **97**, 1538 (1955).
[11]N. S. Averkiev and A. Shik, Phys. Rev. B **59**, 3250 (1999).
[12]A. A. Grinberg and S. Luryi, J. Appl. Phys. **61**, 1181 (1987).
[13]J. Nishizawa, N. Takeda, and F. Masuoka, IEEE Trans. Electron Devices **43**, 2068 (1996), ISSN 0018-9383.
[14]V. Fauske, M. Erlbeck, J. Huh, D. Kim, A. Munshi, D. Dheeraj, H. Weman, B. Fimland, and A. Van Helvoort, J. Microsc. **262**, 183 (2016), ISSN 1365-2818.
[15]F. Léonard, A. A. Talin, B. S. Swartzentruber, and S. T. Picraux, Phys. Rev. Lett. **102**, 106805 (2009).
[16]A. C. E. Chia and R. R. LaPierre, Nanotechnology **22**, 245304 (2011).
[17]E. Latu-Romain, P. Gilet, P. Noel, J. Garcia, P. Ferret, M. Rosina, G. Feuillet, F. Lévy, and A. Chelnokov, Nanotechnology **19**, 345304 (2008).
[18]J. Hu, Y. Liu, C. Z. Ning, R. Dutton, and S.-M. Kang, Appl. Phys. Lett. **92**, 083503 (2008), ISSN 00036951.
[19]H. Ruda and A. Shik, Phys. E (Amsterdam, Neth.) **6**, 543 (2000), ISSN 1386-9477.
[20]K. R. K. Maheswaran and S. Karmalkar, Phys. E (Amsterdam, Neth.) **44**, 700 (2011), ISSN 1386-9477.
[21]A. A. Talin, F. Léonard, A. M. Katzenmeyer, B. S. Swartzentruber, S. T. Picraux, M. E. Toimil-Molares, J. G. Cederberg, X. Wang, S. D. Hersee, and A. Rishinaramangalum, Semicond. Sci. Technol. **25**, 024015 (2010).
[22]A. Katzenmeyer, F. Léonard, A. A. Talin, M. Toimil-Molares, J. G. Cederberg, J. Y. Huang, and J. L. Lensch-Falk, IEEE Trans. Nanotechnol. **10**, 92 (2011), ISSN 1536-125X.
[23]G. Bussone, H. Schäfer-Eberwein, E. Dimakis, A. Biermanns, D. Carbone, A. Tahraoui, L. Geelhaar, P. Haring Bolívar, T. U. Schülli, and U. Pietsch, Nano Lett. **15**, 981 (2015), ISSN 1530-6984.
[24]O. Salehzadeh, K. L. Kavanagh, and S. P. Watkins, J. Appl. Phys. **112**, 054324 (2012), ISSN 00218979.
[25]K. L. Kavanagh, J. Salfi, I. Savelyev, M. Blumin, and H. E. Ruda, Appl. Phys. Lett. **98**, 152103 (2011), ISSN 00036951.
[26]S. A. Dayeh, Semicond. Sci. Technol. **25**, 024004 (2010).